Asian Journal of Chemistry; Vol. 32, No. 10 (2020), 2475-2485

ASIAN JOURNAL OF CHEMISTRY

https://doi.org/10.14233/ajchem.2020.22718

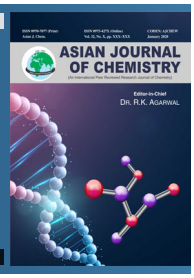

Vibrational Spectroscopic Analysis of 10*H*-Dibenzo[*b*,*e*][2,4]oxazine and Investigate their Structural Reactivity by DFT Computations and Molecular Docking Analysis

M. Latha Beatrice[1,2], S. Mary Delphine[2], M. Amalanathan[3,*] and H. Marshan Robert[4]

[1]Research Scholar, Reg No. 12600, Manonmaniam Sundaranar University, Abishekapatti, Tirunelveli-627 012, India
[2]Department of Physics & Research Centre, Holy Cross College, Nagercoil-629002, India
[3]Department of Physics & Research Centre, Nanjil Catholic College of Arts and Science Kaliyakkavilai-629153, India
[4]Research Scholar, Reg No. 17233282131011, Department of Physics &Research Centre,Women's Christian College, Nagercoil-629001, India

*Corresponding author: E-mail: nathan.amalphysics@gmail.com

Received: 11 March 2020; *Accepted*: 22 May 2020; *Published online*: 25 September 2020; AJC-20056

The molecular structure and vibrational spectra of 10*H*-dibenzo[*b*,*e*][2,4]oxazine was calculated with the help of B3LYP density functional theory (DFT) using 6-311G (d,p) basis set. The FT-IR and FT-Raman spectra of title compound were interpreted by comparing the experimental results with the theoretical B3LYP/6-311G (d,p) calculations. The experimental observed vibrational frequencies are compared with the calculated vibrational frequencies and they are in good agreement with each other. Natural bond orbital (NBO) analysis interprets the intramolecular contacts of title molecule. The ^{1}H and ^{13}C NMR chemical movements of the particle have been determined by the gauge independent atomic orbital (GIAO) strategy and contrasted with the experimental outcome. The deciphered HOMO and LUMO energies showed the chemical stability of the molecules. Fukui capacity and natural charge investigation on atomic charges of the title molecule have been discussed. Docking reads were performed for title molecule utilizing the molecular docking programming with fungicidal dynamic PDB's.

Keywords: Oxazine, DFT, Vibrational analysis, NMR, Molecular docking.

INTRODUCTION

Present day society is subjected to engineered heterocycles for use as medications, pesticides and colours. The most common heterocycles are those having five- or six-membered rings and containing heteroatoms of nitrogen, oxygen or sulfur. The structure of 10*H*-dibenzo[*b*,*e*][2,4]oxazine consists of an oxazine fused to two benzene rings. It occurs as the central core of a number of naturally occurring chemical compounds such as dactinomycin [1]. The 10*H*-dibenzo[*b*,*e*][2,4]oxazine framework is a chromophoric part of the atomic structures of the normally happening actinomycin antitoxins, which are yellow-red in colour. Numerous polycyclic compounds containing a 10*H*-dibenzo-[*b*,*e*][2,4]oxazine ring are utilized as natural stains, texture colours and light-producing materials in colour lasers [1]. Oxazine heterocycles have uncommon intrigue since they establish a significant class of characteristic and non-common items and show helpful biological activities [2]. Oxazine derivatives are a significant class of heterocycles, which has generated a lot of engineered enthusiasm because of their wide scope of natural exercises. Oxazine and related heterocyclic compounds were accounted for to have antimycobacterial, antibacterial, antifungal, anticoagulant, anticancer, cancer prevention agent and cytotoxic exercises. Oxazine obtained from benzene and its reduced form, by substitution of carbon (and hydrogen) atoms by nitrogen and oxygen. Over the most recent couple of years oxazine derivatives have been considered as significant engineered intermediates and furthermore have significant organic exercises like soothing, pain relieving, antipyretic, anti-convulsant, antitubercular, anti-tumour, antimalarial and antimicrobial [3].

In the present study, vibrational spectroscopic analysis of 10*H*-dibenzo[*b*,*e*][2,4]oxazine (10HXZ) are reported experimentally and theoretically. A complete vibrational spectroscopic investigation of the 10HXZ molecule to give a brief assignment of the fundamental bands in FT-IR and FT-Raman

spectra on the basis of normal coordinate analysis. The straight connection between the scale factor and the vibrational wavenumbers are related to the assistance of the wavenumber linear scaling (WLS) strategy. The redistribution of electron density (ED) in different bonding and antibonding orbitals alongside E (2) energies have been determined by normal bond orbital (NBO) utilizing B3LYP/6-311G (d,p) basis set. A few properties like highest occupied molecular orbital (HOMO), lowest unoccupied molecular orbital (LUMO), MESP and global reactive descriptors are done to give data about charge move inside the compound. The chemical shifts 10HXZ molecule is predicted from NMR spectrum. The microbial activity of 10HXZ molecule is discussed by molecular docking. The present study provides complete information about spectral, structural, chemical and microbial activity of 10HXZ compound.

COMPUTATIONAL METHODS

The 10HXZ molecule is theoretically optimized DFT method at B3LYP/6-311G(d,p) basis set to using Gaussian 09W programs [4]. The detailed vibrational spectra of 10HXZ molecule can be determined with the help of normal coordinate analysis (NCA). Normal coordinate analysis was performed utilizing the MOLVIB program version 7.0 composed by Sundius [5]. The wavenumbers acquired from Normal coordinate analysis technique were downsized by the (WLS) wavenumber linear scaling strategy [6]. The natural bond orbitals (NBO) figurings [7] were performed utilizing NBO 3.1 program as actualized in the Gaussian 09W bundle at DFT/B3LYP level. ^{1}H and ^{13}C NMR isotropic shielding were calculated by GIAO method [8] using optimized parameters obtained from B3LYPwith 6-311G (d,p) method. AutoDock4 (version 4.2) with the Lamarckian genetic algorithm was used to perform docking studies [9].

EXPERIMENTAL

The compound 10HXZ in the solid form was bought from sigma Aldrich chemical company (USA) with a stated purity of greater than 97% and it was used as such without further purification. The Fourier Transform infrared (FTIR) range of this compound was recorded in the area 4000-450 cm^{-1} on a Bruker model IFS 66V spectrophotometer utilizing KBr pellet procedure. The FT-Raman range was likewise recorded in FT-Raman BRUKER RFS 100/s instrument outfitted with Nd: YAG laser source working at 1064 nm frequency and 150 mw powers in the range 4000-100 cm^{-1}. The ^{1}H and ^{13}C NMR spectra are taken in methonal solutions and all signals are referenced to TMS on a BRUKER AVANCE III500 MHz (AV500) spectrometer. The spectral measurements were done at Regional Sophisticated Instrumentation Centre, IIT, Chennai, Tamil Nadu, India.

RESULTS AND DISCUSSION

Optimized geometry: The molecule 10HXZ molecular structure and atom numbering is shown in Fig. 1. The optimized parameters of 10HXZ molecule are listed in Table-1. The optimized values are compared with X-ray diffraction results [10,11]. The 10HXZ calculated C-C bond lengths are

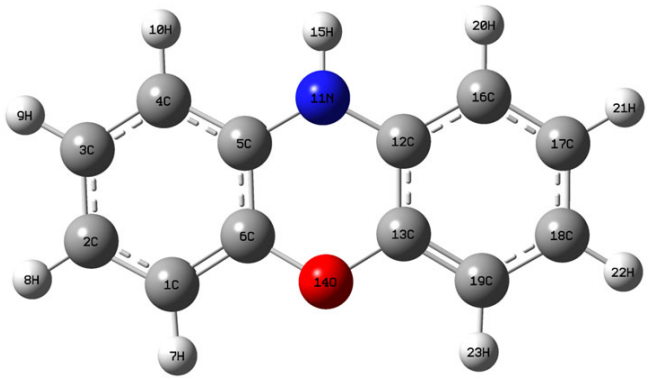

Fig. 1. Optimized structure of 10HXZ molecule optimized at B3LYP/6-311 G(d,p) basis set

almost agreed with the experimental C-C bond lengths. The C-C bond lengths of 10HXZ are not in same length. The calculated C-C bond length values of 10HXZ are varied between 1.3841-1.4037 Å and the experimental values are varied between 1.379-1.402 Å. From the Table-1, C_5-C_6 and C_{12}-C_{13} bond length shows greater value due to the presence of neighboring nitrogen and oxygen atom and its range belongs to 1.40 and the lower range is for C_2-C_3 and C_{13}-C_{19} which is 1.384. The experimental and calculated C-N bond lengths are lie in the range 1.39 Å and 1.40 Å, whereas these bond lengths are much shorter than the normal C-N (1.49 Å) single bond [12] which confirms these bonds have some character of a double or conjugate bond. The calculated C-O bond length (1.384 Å) agreed with the experimental C-O (1.389 Å) bond length value. The N_{11}-H_{15} bond length of the compound is 0.860 (XRD), 1.0077 Å (DFT). Dandia *et al*. [13] reported this value as 0.80 Å. The C_{12}-N_{11}-C_5, C_5-N_{11}-H_{15} and C_{12}-N_{11}-H_{15} bond angle of the 10HXZ molecule for DFT (XRD) are 119.73 (124.06), 117.48 (117.9) and 117.48 (118.05). The asymmetry of the bond angle values is due to the interaction of N_{11}-H_{15} with hydrogen atoms H_{10} and H_{20}.

The computational and experimental dihedral angles of the 10HXZ are C_3-C_4-C_5-N_{11} = 178.47 (B3LYP), -177.23 (XRD); C_4-C_5-N_{11}-C_{12} = -166.87 (B3LYP), 169.67 (XRD); C_2-C_1-C_6-O_{14} = 178.36 (B3LYP), -177.56 (XRD); C_1-C_6-O_{14}-C_{13} = -167.07 (B3LYP), -170.99 (XRD); C_{18}-C_{19}-C_{13}-O_{14} = -178.36 (B3LYP), 179.37 (XRD); C_{19}-C_{13}-O_{14}-C_6 = -167.07 (B3LYP), 170.64 (XRD); C_{17}-C_{16}-C_{12}-N_{11} = 178.47 (B3LYP), -178.61 (XRD); C_{16}-C_{12}-N_{11}-C_5 = 166.87 (B3LYP), -169.28 (XRD); and these values declare the little boat conformation for the oxazine ring with respect to the phenyl rings.

Vibrational analysis: The molecular structure of 10HXZ molecule comprises of 23 atoms, indicating a total number of 63 normal modes of vibrations which are assigned by using PED. Most of the observed vibrational patterns concur with hypothetically determined vibrational modes. Both experimental and theoretical FT-IR, FT-Raman spectra of 10HXZ molecule are shown in Figs. 2 & 3 and vibrational frequencies are furnished in Table-2.

NH vibration: The NH modes are expected in the range 3500-3000 cm^{-1} (stretching) and around 1500 cm^{-1} (deformation) [14-16]. In 10HXZ, a strong band observed at 3396 cm^{-1} in IR

TABLE-1
OPTIMIZED GEOMETRIC PARAMETERS OF 10HXZ MOLECULE ON B3LYP/6-311G (d,p) BASIS SET

Bond length	Values (Å)		Bond angle	Values (°)		Dihedral angle	Values (°)	
	Cal.	Exp.		Cal.	Exp.		Cal.	Exp.
C_1-C_2	1.3972	1.387	C_1-C_2-C_3	119.6769	119.62	C_1-C_2-C_3-C_4	-0.150	0.53
C_2-C_3	1.3896	1.384	C_2-C_3-C_4	120.1823	120.46	C_2-C_3-C_4-C_5	-0.372	1.05
C_3-C_4	1.3956	1.394	C_3-C_4-C_5	120.5404	120.44	C_3-C_2-C_1-C_6	0.581	-1.21
C_5-C_6	1.4037	1.400	C_2-C_1-C_6	120.0513	119.95	C_5-C_6-C_1-H_7	179.88	-179.73
C_1-C_6	1.3841	1.379	C_6-C_1-H_7	118.3145	120.01	C_6-C_1-C_2-H_8	-179.56	178.80
C_1-H_7	1.0832	0.950	C_1-C_2-H_8	119.7525	120.16	C_1-C_2-C_3-H_9	179.84	-179.45
C_2-H_8	1.0831	0.950	C_2-C_3-H_9	120.3735	119.73	C_2-C_3-C_4-H_{10}	-179.85	-179.00
C_3-H_9	1.0835	0.951	C_3-C_4-H_{10}	120.3083	119.74	C_3-C_4-C_5-N_{11}	-178.47	177.23
C_4-H_{10}	1.0853	0.950	C_4-C_5-N_{11}	122.8062	122.75	C_4-C_5-N_{11}-C_{12}	-166.87	169.67
C_5-N_{11}	1.3974	1.407	C_5-N_{11}-C_{12}	119.7328	118.99	C_5-N_{11}-C_{12}-C_{13}	-14.19	11.40
C_{12}-N_{11}	1.3974	1.404	N_{11}-C_{12}-C_{13}	118.4392	119.17	C_2-C_1-C_6-O_{14}	178.36	-177.56
C_{12}-C_{13}	1.4037	1.402	C_1-C_6-O_{14}	117.9823	117.10	C_4-C_5-N_{11}-H_{15}	-13.18	11.04
C_6-O_{14}	1.3842	1.389	C_5-N_{11}-H_{15}	117.4896	117.90	C_5-N_{11}-C_{12}-C_{16}	166.87	-169.28
N_{11}-H_{15}	1.0077	0.860	N_{11}-C_{12}-C_{16}	122.8062	122.80	N_{11}-C_{12}-C_{16}-C_{17}	178.47	-178.61
C_{12}-C_{16}	1.394	1.390	C_{12}-C_{16}-C_{17}	120.5404	120.59	C_{12}-C_{16}-C_{17}-C_{18}	0.372	0.06
C_{16}-C_{17}	1.3956	1.387	C_{16}-C_{17}-C_{18}	120.1823	120.80	N_{11}-C_{12}-C_{13}-C_{19}	-178.95	178.12
C_{17}-C_{18}	1.3896	1.379	C_{12}-C_{13}-C_{19}	120.7993	121.27	N_{11}-C_{12}-C_{16}-H_{20}	-1.022	1.38
C_{13}-C_{19}	1.3841	1.379	C_{12}-C_{16}-H_{20}	119.1493	119.68	C_{12}-C_{16}-C_{17}-H_{21}	-179.63	-180.00
C_{16}-H_{20}	1.0853	0.949	C_{16}-C_{17}-H_{21}	119.4441	119.58	C_{16}-C_{17}-C_{18}-H_{22}	-179.99	179.71
C_{17}-H_{21}	1.0835	0.950	C_{17}-C_{18}-H_{22}	120.5705	120.32	C_{12}-C_{13}-C_{19}-H_{23}	-179.88	-179.03
C_{18}-H_{22}	1.0831	0.950	C_{13}-C_{19}-H_{23}	118.3145	120.09	C_1-C_6-O_{14}-C_{13}	167.07	-170.99
C_{19}-H_{23}	1.0832	0.950	C_{12}-N_{11}-H_{15}	117.480	118.05	C_{18}-C_{19}-C_{13}-O_{14}	-178.36	179.37
C_{13}-O_{14}	1.3842	1.389	C_{12}-N_{11}-C_5	119.730	124.06	C_{19}-C_{13}-O_{14}-C_6	-167.07	170.64

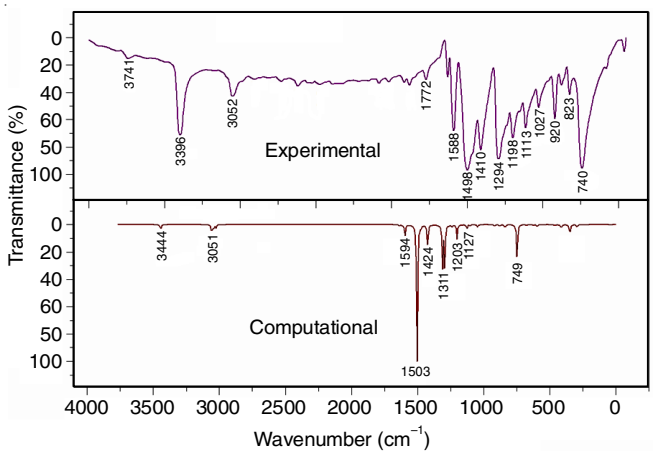

Fig. 2. Combined FT-IR spectrum of 10HXZ molecule

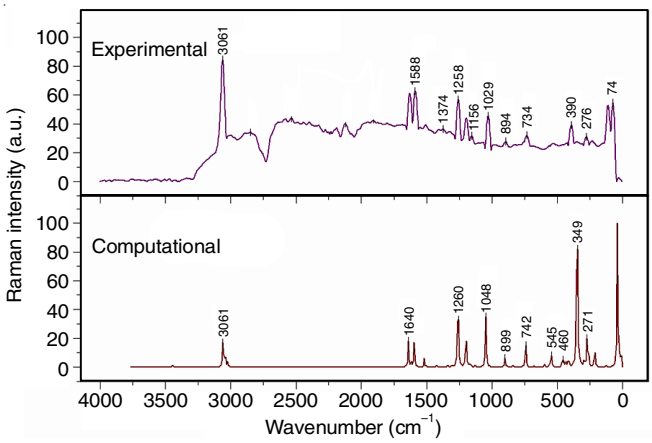

Fig. 3. Combined FT-Raman spectrum of 10HXZ molecule

TABLE-2
COMPARISON OF THE EXPERIMENTAL (FT-IR, FT-RAMAN) WAVENUMBERS (cm^{-1}) AND THEORETICAL WAVENUMBERS (cm^{-1}) OF 10HXZ MOLECULE CALCULATED BY B3LYP/6-311G (d,p) LEVEL OF THEORY

Wavenumbers			IR intensity	Raman intensity	Assignments with PED (%)
Experimental values		Calculated values			
FT-IR	FT-Raman				
3396 vs	-	3444	4.09674	1.06895	$\nu N_{11}H_{15}$(100)
-	3061 vs	3061	0.55512	6.1804	νCH_{PH2}(50), νCH_{PH1}(49)
-	-	3060	2.82725	0.2782	νCH_{PH1}(50), νCH_{PH2}(49)
3052 m	-	3051	1.72868	2.66384	νCH_{PH1}(50), νCH_{PH2} (49)
-	-	3050	3.56295	0.3827	νCH_{PH2}(50), νCH_{PH1}(49)
-	-	3040	1.87697	0.64568	νCH_{PH2}(50), νCH_{PH1}(49)
-	-	3039	0.02027	1.83698	νCH_{PH1}(50), νCH_{PH2}(49)
-	-	3024	2.27438	1.59624	νCH_{PH1}(50), νCH_{PH2}(49)
-	3000 w	3023	0.59697	0.00341	νCH_{PH2}(50), νCH_{PH1}(49)
1628 m	1630 s	1640	0.82638	4.69462	νCC_{PH1}(32), νCC_{PH2}(28), δCCN(7), βCCH_{PH1}(6), βCCH_{PH2}(6), δCCC_{PH1}(6)

-	-	1617	0.2305	0.80277	$\nu CC_{PH1}(33)$, $\nu CC_{PH2}(33)$, $\delta CCC_{PH2}(5)$, $\delta CCC_{PH1}(5)$, $\beta CCH_{PH1}(5)$
-	-	1606	0.97902	0.10309	$\nu CC_{PH1}(34)$, $\nu CC_{PH2}(34)$, $\beta CNH(9)$, $\delta CCC_{PH2}(6)$, $\beta CCH_{PH2}(5)$
1588s	1588s	1594	7.90107	4.35886	$\nu CC_{PH1}(30)$, $\nu CC_{PH2}(30)$, $\beta CCH_{PH1}(7)$, $\beta CCH_{PH2}(7)$, $\delta CCN(6)$, $\nu CN(5)$
-	-	1519	0.27101	1.52313	$\beta CCH_{PH2}(21)$, $\beta CCH_{PH1}(21)$, $\nu CC_{PH1}(21)$, $\nu CC_{PH2}(17)$, $\nu CN(8)$, $\nu CO(5)$
-	1509 w	1507	12.72074	0.01804	$\beta CNH(23)$, $\beta CCH_{PH1}(19)$, $\beta CCH_{PH2}(19)$, $\nu CC_{PH1}(15)$, $\nu CC_{PH2}(13)$
1498 m	-	1502	100	0.01344	$\nu CN(28)$, $\nu CC_{PH1}(17)$, $\nu CC_{PH2}(12)$, $\beta CCH_{PH1}(10)$, $\beta CCH_{PH2}(10)$, $\beta CNH(9)$
-	-	1472	1.18997	0.04431	$\beta CCH_{PH1}(24)$, $\beta CCH_{PH2}(24)$, $\nu CC_{PH1}(20)$, $\nu CC_{PH2}(20)$, $\delta CCN(10)$
1410 m	1406vw	1424	19.70371	0.34168	$\beta CCH_{PH2}(23)$, $\beta CCH_{PH1}(23)$, $\beta CNH(16)$, $\nu CC_{PH2}(12)$, $\nu CC_{PH1}(12)$, $\nu CN(6)$
-	1374 w	1340	0.39754	0.29338	$\nu CC_{PH1}(43)$, $\nu CC_{PH2}(43)$
-	-	1311	30.76201	0.05885	$\nu CC_{PH1}(38)$, $\nu CC_{PH2}(38)$, $\nu CN(8)$, $\beta CCH_{PH2}(7)$, $\beta CCH_{PH1}(7)$
-	-	1300	0.00652	0.06711	$\beta CCH_{PH1}(36)$, $\beta CCH_{PH2}(36)$, $\delta CCN(19)$
1294 m	-	1295	30.97402	0.03855	$\nu CO(18)$, $\beta CCH_{PH2}(17)$, $\beta CCH_{PH1}(17)$, $\nu CC_{PH1}(13)$, $\nu CC_{PH2}(13)$, $\nu CN(10)$
-	1258 s	1260	0.39797	14.9248	$\nu CN(38)$, $\nu CC_{PH1}(14)$, $\nu CC_{PH2}(11)$, $\beta CCH_{PH1}(11)$, $\beta CCH_{PH2}(11)$, $\delta CCC_{PH1}(5)$
-	-	1241	1.50216	0.02306	$\beta CNH(18)$, $\nu CC_{PH1}(16)$, $\beta CCH_{PH2}(14)$, $\beta CCH_{PH1}(14)$, $\nu CC_{PH2}(13)$, $\delta CCN(9)$
-	1200 m	1203	10.50757	0.78765	$\nu CO(37)$, $\nu CN(13)$, $\beta CCH_{PH2}(10)$, $\beta CCH_{PH1}(10)$, $\delta CCC_{PH1}(8)$, $\delta CCC_{PH2}(8)$
1198 m	-	1197	0.65846	5.61628	$\nu CO(38)$, $\delta CCC_{PH1}(14)$, $\delta CCC_{PH2}(14)$, $\nu CC_{PH1}(9)$, $\nu CC_{PH2}(8)$
-	1156 w	1168	0.16257	0.582	$\beta CCH_{PH2}(42)$, $\beta CCH_{PH1}(42)$, $\nu CC_{PH1}(8)$, $\nu CC_{PH2}(8)$
-	-	1165	0.05876	0.04823	$\beta CCH_{PH1}(40)$, $\beta CCH_{PH2}(40)$, $\nu CC_{PH1}(10)$, $\nu CC_{PH2}(10)$
1113 m	-	1127	3.38939	0.15677	$\beta CCH_{PH2}(26)$, $\beta CCH_{PH1}(26)$, $\nu CC_{PH1}(14)$, $\nu CC_{PH2}(13)$, $\delta CCC_{PH2}(5)$, $\delta CCC_{PH1}(5)$
-	-	1103	0.61518	0.00315	$\nu CC_{PH1}(17)$, $\nu CC_{PH2}(17)$ $\beta CCH_{PH1}(15)$, $\beta CCH_{PH2}(15)$, $\delta CCC_{PH1}(11)$, $\delta CCC_{PH2}(11)$
-	-	1048	1.84483	0.01946	$\nu CC_{PH1}(34)$, $\nu CC_{PH2}(33)$, $\beta CCH_{PH2}(16)$, $\beta CCH_{PH1}(16)$
1027 m	1029 s	1046	0.04275	8.01679	$\nu CC_{PH1}(36)$, $\nu CC_{PH2}(36)$, $\beta CCH_{PH1}(13)$, $\beta CCH_{PH2}(13)$
-	-	952	0.01095	0.00764	$\omega CCHC_{PH1}(45)$, $\omega CCHC_{PH2}(45)$
920 s	-	951	0.00087	0.00981	$\omega CCHC_{PH2}(45)$, $\omega CCHC_{PH1}(45)$
-	-	917	1.46749	0.03291	$\omega CCHC_{PH1}(45)$, $\omega CCHC_{PH2}(45)$
-	-	916	0.02353	0.1683	$\omega CCHC_{PH2}(45)$, $\omega CCHC_{PH1}(45)$
-	894 w	899	0.00611	1.22543	$\delta CCC_{PH2}(30)$, $\delta CCC_{PH1}(30)$, $\nu CN(11)$, $\nu CO(11)$
877 w	-	880	1.16844	0.10926	$\delta COC(23)$, $\delta CCC_{PH1}(22)$, $\delta CCC_{PH2}(22)$, $\nu CO(8)$, $\nu CN(7)$
-	-	841	2.22297	0.11203	$\nu CC_{PH1}(27)$, $\nu CC_{PH2}(27)$, $\nu CO(11)$, $\omega CCHC_{PH1}(9)$, $\omega CCHC_{PH2}(9)$
-	-	840	0.03073	0.40494	$\omega CCHC_{PH2}(43)$, $\omega CCHC_{PH1}(43)$
823 m	-	837	0.38347	0.04059	$\omega CCHC_{PH2}(40)$, $\omega CCHC_{PH1}(40)$
-	-	750	0.28681	0.00201	$\omega CCHC_{PH2}(48)$, $\omega CCHC_{PH1}(48)$
-	-	749	22.16407	0.28323	$\omega CCHC_{PH1}(44)$, $\omega CCHC_{PH2}(43)$
740 s	734 w	742	2.62347	3.20809	$\nu CC_{PH1}(16)$, $\nu CO(13)$, $\delta CCC_{PH2}(12)$, $\delta CCC_{PH1}(12)$, $\nu CC_{PH2}(12)$, $\delta CCC_{PH2}(10)$
-	-	719	0.01009	0.0085	$\pi CCCC_{PH1}(34)$, $\pi CCCC_{PH2}(31)$, $\pi CCNC(16)$, $\omega CCHC_{PH1}(6)$, $\omega CCHC_{PH2}(6)$
-	-	691	0.02665	0.01652	$\pi CCCC_{PH1}(39)$, $\pi CCCC_{PH2}(35)$, $\omega CCHC_{PH1}(7)$, $\omega CCHC_{PH2}(7)$, $\tau CCNC(6)$
-	-	681	0.32259	0.17987	$\delta CCN(33)$, $\delta CCC_{PH1}(18)$, $\delta CCC_{PH2}(12)$, $\nu CC_{PH1}(8)$, $\nu CC_{PH2}(8)$
-	-	624	0.44051	0.05126	$\delta CCC_{PH2}(55)$, $\delta CCC_{PH1}(36)$
578 vw	-	597	1.52547	0.51253	$\delta CCC(39)$, $\delta CCC_{PH2}(29)$, $\delta CCC_{PH1}(15)$
-	539 vw	561	0.07559	0.22589	$\tau CCCC_{PH2}(25)$, $\pi CCNC(16)$, $\tau CCCC_{PH1}(15)$, $\pi CCCC_{PH1}(10)$, $\pi CCCC_{PH2}(9)$
-	-	557	0.000155	0.16691	$\tau CCCC_{PH2}(30)$, $\tau CCCC_{PH1}(26)$, $\omega CCHC_{PH2}(8)$, $\omega CCHC_{PH1}(8)$
-	532vw	545	0.10803	1.82055	$\delta CCC_{PH1}(37)$, $\delta CCC_{PH2}(33)$, $\delta CCN(7)$
460 m	-	460	0.67722	1.20524	$Butterfly_{PH1}(21)$, $Butterfly_{PH2}(21)$, $\tau CCCC_{PH2}(20)$, $\tau CCCC_{PH1}(17)$
-	-	449	0.00504	0.63012	$\tau CCCC_{PH1}(28)$, $\tau CCCC_{PH2}(27)$, $Butterfly_{PH1}(19)$, $Butterfly_{PH2}(19)$
-	-	431	0.24664	0.8705	$\delta CCN(80)$, $\nu CC_{PH1}(6)$, $\nu CC_{PH2}(6)$,
-	390 m	413	3.48202	1.5427	$\beta CNH(27)$, $\nu CN(22)$, $\nu CC_{PH1}(7)$, $\nu CC_{PH2}(7)$, $\delta CCC_{PH2}(6)$, $\nu CN(6)$
-	-	349	9.44885	33.556	$\beta CNH(62)$, $\delta CCN(15)$
-	276 w	295	2.19229	1.0922	$\tau CCCC_{PH2}(13)$, $\tau CCOC(12)$, $Butterfly_{PH2}(11)$, $Butterfly_{PH1}(11)$, $\tau CCCC_{PH1}(10)$, $\omega CCHC_{PH1}(9)$
-	-	271	0.0368	6.0984	$Butterfly_{PH1}(19)$, $Butterfly_{PH2}(19)$, $\tau CCCC_{PH1}(14)$, $\omega CCHC_{PH1}(13)$, $\omega CCHC_{PH2}(13)$, $\tau CCCC_{PH2}(12)$
-	237 w	259	0.20316	1.7924	$\pi CCOC(15)$, $\nu CN(11)$, $\delta CCC_{PH2}(10)$, $\delta CCC_{PH1}(8)$, $\nu CO(8)$, $\tau CCCC_{PH2}(8)$
-	184 m	212	0.04794	3.5265	$\pi CCNC(28)$, $\tau CCCC_{PH1}(24)$, $\tau CCCC_{PH2}(20)$
-	109 s	124	0.00189	0.5776	$\tau CCCC_{PH1}(30)$, $\tau CCCC_{PH2}(27)$, $\tau CCNC(27)$
-	74 s	40	0.17757	100	$\tau CCNC(72)$, $\omega CNHC(21)$

vs- very strong, s-strong, w-weak, vw-very weak, m-mediam, ν-stretching, β-in-plane bending, δ-deformation, ω-out-of-plane bending, π-puckering, τ-torsion, PH1-phenyl ring 1, PH2- phenylring 2

spectrum is assigned for NH symmetric stretching with 100% of PED contribution and the compared calculated value for this NH symmetric stretching mode is 3444 cm^{-1}. In IR spectrum, the NH stretching frequency is red shifted by 48 cm^{-1} with a strong intensity from the calculated frequency 3444 cm^{-1}, which indicates weakening of the NH bond resulting in hydrogen ion transfer to the neighbouring units. In the present 10HXZ molecule, the weak C-N-H deformation band is observed at 1509 cm^{-1} in Raman spectrum and the calculated value for this mode is 1507 cm^{-1}.

CH vibration: The phenyl CH stretching vibrations occur above 3000 cm^{-1} and are typically exhibited as multiplicity of weak to moderate bands compared with the aliphatic CH stretching [17]. In this area, the peaks are not disturbed markedly by the nature of the elements. In the present investigation, A very strong band observed in Raman spectrum at 3061 cm^{-1}, medium band is observed in IR spectrum at 3052 cm^{-1} is assigned for C-H stretching vibration and the compared calculated wavenumber is 3061 cm^{-1} (Raman) and 3051 cm^{-1} (IR) with maximum 99% of PED contribution. The experimental C-H stretching wavenumbers are coinciding with the calculated C-H stretching wavenumbers. The C-H in-plane and out of-plane bending vibrations typically occur as various high to low intensity sharp bands in the area of 1300-1000 and 1000-750 cm^{-1} [18] respectively. In this case, the medium bands observed in IR spectrum at 1294, 1113, 1027 cm^{-1} and the strong Raman band observed at 1258, 1029 cm^{-1}, medium Raman band at 1200 cm^{-1}, weak Raman band at 1156 cm^{-1} correspond to C-H in-plane bending vibration, which are mixed with other vibrational modes. The strong band observed in IR spectrum at 920 cm^{-1} and medium band observed in IR spectrum at 823 cm^{-1} is assigned for C-H out of plane bending vibration and the calculated value for this mode is 951 and 837 cm^{-1}.

C-N vibrations: The stretching vibration of C-N modes is occurred in the range 1300-1100 cm^{-1} [19]. In the 10HXZ molecule a strong band observed in the range 1258 cm^{-1} (Raman) is assigned as C-N stretching modes. The compared calculated value for C-N stretching mode is 1260 cm^{-1}. The C-N deformation mode of 10HXZ molecule theoretically observed at 431 cm^{-1} (DFT) with 80% PED contribution and one medium band found at 184 cm^{-1} (Raman) is assigned for C-N out-of-plane bending vibration with 28 percentage minimum contribution of PED.

C-C vibrations: Most of the ring vibrational modes are affected by the substitutions in the ring of the 10HXZ molecule. The *ortho* substituted phenyl stretching modes are expected in the range 1615-1260 cm^{-1} [20]. Two strong bands are observed at 1630, 1588 cm^{-1} in Raman spectrum and one medium and strong band observed at 1628, 1588 cm^{-1} in IR spectrum is assigned for phenyl ring stretching modes. The compared calculated value for this stretching mode is 1640, 1594 cm^{-1} respectively. In present work, strong band observed at 740 cm^{-1} in FT-IR spectrum and weak band at 734 cm^{-1} in FT-Raman spectrum is allotted for phenyl ring bending vibrations and the corresponding calculated value for this mode is 742 cm^{-1} in the molecule under analysis. The out-of plane and in-plane bending C-C-C modes of 10HXZ molecule are presented in Table-2. Theoretically the band determined at 1048 cm^{-1} is assigned as the ring breathing mode of *ortho* subbed phenyl ring. Kaur *et al*. [21] reported the ring breathing mode of *ortho* subbed benzene rings at 1026 and 1023 cm^{-1} theoretically.

C-O vibration: Usually, the bands at 1200-1300 cm^{-1} are assigned to C-O stretching vibrations for substituted phenol [22]. In the present study, medium band observed at 1200-1198 cm^{-1} in FT-IR and FT-Raman spectrum is assigned for C-O stretching vibration, the compared calculated value for C-O stretching mode is 1203-1197 cm^{-1}. The C-O in-plane bending vibrations are observed at 877 cm^{-1} in FT-IR spectrum and theoretically computed value at 880 cm^{-1} show good agreement with experimental observations. The medium to weak band are observed in Raman spectrum at 276, 237 and 184 cm^{-1} as C-O out-of-plane bending vibrations and the compared theoretical values are 295, 259, 212 cm^{-1}.

Natural bond orbital analysis: The natural bond orbital (NBO) analysis was performed at the B3LYP/6-311G(d,p) level basis set. The stabilizing interactions between filled and unoccupied orbital's and destabilizing interactions between filled orbital's can be obtained from this analysis [23-25]. Various second order interactions between the filled and unoccupied orbitals are investigated using DFT level computation which gives a measure of the delocalization or hyper conjugation. NBO analysis provides the most accurate possible 'natural Lewis structure' picture of j, because all orbital details are mathematically chosen to include the highest possible percentage of the electron density. Delocalization of electron density between occupied Lewis-type (bond or lone pair) NBO orbital's and formally unoccupied (antibond) non-Lewis NBO orbital's corresponds to a stabilizing donor-acceptor interaction. The NBO method also gives information about interactions in both filled and virtual orbital spaces that could enhance the analysis of intra- and intermolecular interactions [23,26]. The interactions due to electron delocalization are generally analyzed by selecting a number of bonding and antibonding NBO's. For each donor NBO (i) and accepter NBO (j) the stabilization energy E(2) is associated with i→j delocalization is given by the following equation:

$$E(2) = \Delta E_{ij} = q_i F(i,j)^2/\Sigma j\text{-}\Sigma i$$

where, q_i is the donor orbital occupancy, Σi and Σj are diagonal elements and F(i,j) is the off diagonal NBO Fock matrix element. The second-order perturbation theory analysis of Fock matrix in NBO basis is given in Table-2. In NBO analysis large E(2) value shows the intensive interaction between electron-donors and electron-acceptors and greater the extent of conjugation of the whole system [27]. The important donor-acceptor Interactions of 10HXZ compound are given in Table-3. The intramolecular hyper-conjucative interaction is formed by an orbital overlap between π(C–C), σ(C–C) and π*(C–C), σ*(C–C) bond orbital which results in intra-molecular charge transfer causing the system to stabilize.

The electron density of the phenyl ring (1.6 to 1.9e) show strong charge delocalization. The important interaction energy in this molecule, is electron donating from $\sigma(C_{18}\text{-}C_{19})$ to the antibonding $\sigma^*(C_{19}\text{-}H_{23})$ and another one electron donating

TABLE-3
SECOND ORDER PERTURBATION THEORY ANALYSIS OF FOCK MATRIX OF 10HXZ MOLECULE BY NBO METHOD

Donar (NBO)	E.D(i)	Acceptor (NBO)	E.D(j)	E^2 (Kcal/mol)	E_j-E_i (a.u)	$F_{i,j}$ (a.u)
$\pi(C_1-C_6)$	1.69332	$\sigma^*(C_{17}-C_{18})$	0.01620	55.07	0.04	0.045
$\sigma(C_1-H_7)$	1.97542	$\sigma^*(C_{17}-C_{18})$	0.01620	14.24	0.29	0.058
$\sigma(C_6-O_{14})$	1.98878	$\sigma^*(C_{17}-C_{18})$	0.01620	84.06	0.67	0.213
$\sigma(C_6-O_{14})$	1.98878	$\sigma^*(C_{19}-H_{23})$	0.01263	53.35	1.56	0.257
$\pi(C_{12}-C_{16})$	1.68188	$\pi^*(C_{17}-C_{18})$	0.34852	65.56	0.04	0.051
$\sigma(C_{13}-C_{19})$	1.97340	$\sigma^*(N_{11}-C_{12})$	0.02442	39.46	0.93	0.071
$\sigma(C_{13}-C_{19})$	1.97340	$\sigma^*(C_{13}-C_{19})$	0.01904	160.70	0.90	0.340
$\sigma(C_{13}-C_{19})$	1.97340	$\sigma^*(C_{17}-C_{18})$	0.01620	292.91	0.54	0.355
$\sigma(C_{13}-C_{19})$	1.97340	$\pi^*(C_{17}-C_{18})$	0.34852	129.11	2.10	0.507
$\sigma(C_{13}-C_{19})$	1.97340	$\sigma^*(C_{19}-H_{23})$	0.01263	119.20	1.42	0.369
$\sigma(C_{18}-C_{19})$	1.97303	$\sigma^*(C_{13}-C_{19})$	0.01904	115.13	0.89	0.286
$\sigma(C_{18}-C_{19})$	1.97303	$\sigma^*(C_{17}-C_{18})$	0.01620	235.03	0.53	0.316
$\sigma(C_{18}-C_{19})$	1.97303	$\pi^*(C_{17}-C_{18})$	0.34852	129.45	2.09	0.507
$\sigma(C_{18}-C_{19})$	1.97303	$\sigma^*(C_{19}-H_{23})$	0.01263	298.88	1.41	0.582
$\sigma(C_{19}-H_{23})$	1.97635	$\sigma^*(N_{11}-C_{12})$	0.02442	160.35	0.26	0.181
$\sigma(C_{19}-H_{23})$	1.97635	$\sigma^*(C_{13}-C_{19})$	0.01904	260.02	0.22	0.214
$\sigma(C_{19}-H_{23})$	1.97635	$\sigma^*(C_{19}-H_{23})$	0.01263	202.11	0.74	0.347
LP(1) N_{11}	1.74780	π^* $(C_{12}-C_{16})$	0.40259	34.17	0.32	0.097
LP(1) N_{11}	1.74780	$\sigma^*(C_{13}-C_{19})$	0.01904	25.44	0.44	0.100
LP(1) N_{11}	1.74780	$\sigma^*(C_{17}-C_{18})$	0.01620	343.83	0.08	0.154
LP(1) N_{11}	1.74780	$\sigma^*(C_{19}-H_{23})$	0.01263	50.45	0.96	0.209
LP(1) O_{14}	1.96311	$\pi^*(C_1-C_6)$	0.36848	22.70	0.35	0.084

from $\sigma(C_{13}-C_{19})$ to the antibonding $\sigma^*(C_{17}-C_{18})$ resulting stabilization of 298.88, 292.91 kcal/mol. The most important interaction (n-π^*) and (n-σ^*) energies of lone pair O_{14} to $\pi^*(C_1–C_6)$ and lone pair N_{11} $\sigma^*(C_{17}–C_{18})$ are 22.70 and 343.83 kcal/mol, respectively. This larger E(2) value reveals the strong ICT interactions of this molecule. The interaction between the bonding and antibonding orbitals are observed as an increase in (electron density) electron density of C-C orbital that weakens the respective bonds. There arise a strong intramolecular hyperconjugative interaction of C_{12}-C_{16} from N_{11} of LP1 (N_{11})-π^* (C_{12}-C_{16}) which increases electron density (0.40259e) that weakens the respective bonds C_{12}-C_{16} leading to stabilization of 34.17 kcal/mol. The strong intramolecular hyperconjugative interaction of lone pair N_{11} to anti bonding $\sigma^*(C_{19}-H_{23})$ atoms increases electron density (0.01263e) that weakens the respective bond C_{19}-H_{23} leading to stabilization of 50.45 kcal/mol of the system. The above higher energy E(2) value for the bonding and antibonding interaction of the title molecule tend to system stabilization.

HOMO-LUMO analysis: To demonstrate some type of interaction and find out the highest reactive part of conjugated molecules, MOs and their properties are used [28]. HOMO and LUMO are the most important orbital in a molecule. Highest occupied molecular orbital containing electrons in an outer orbital tend to act as an electron donor, thus the ionization potential directly connected with the energy of HOMO. In other side, lowest unoccupied MOs ready to accept an electron and the energy of LUMO is directly associated with electron affinity of the molecule [29]. HOMO and LUMO type of molecular orbital in 10HXZ molecule are plotted in Fig. 4. In the 10HXZ molecule, the π nature of HOMO is delocalized over the phenyl rings and oxazine ring except phenyl rings hydrogen

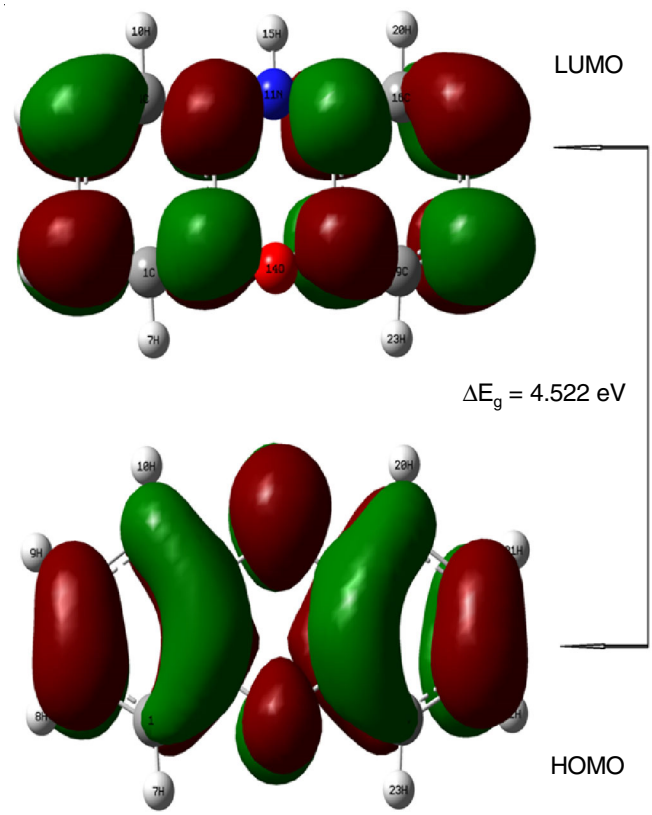

Fig. 4. HOMO-LUMO plot of 10HXZ molecule on B3LYP/6-311G(d,p) basis set

atom. From the molecular orbitals plot LUMO is located over the entire structure except oxazine ring oxygen and NH group. Oxazine ring nitrogen and oxygen atom involve charge transfer interaction within the molecule in both HOMO and LUMO

state, which suggest oxazine ring is the active site of the title molecule. Using HOMO and LUMO orbital energies, the ionization energy and electron affinity can be expressed as: $I = -E_{HOMO}$, $A = -E_{LUMO}$, $\eta = (-E_{HOMO} + E_{LUMO})/2$ and $\mu = 1/2(E_{LUMO} + E_{HOMO})$ [30]. The global electrophilicity power of a molecule as $\omega = \mu^2/2\eta$ is initiated by Parr *et al*. [31]. The stabilization in energy may measured by the electrophilicity index when the molecule acquires an additional electronic charge from the environment. The ability of an electrophile and the resistance of the system are related to the electrophilicity index of the molecule. It contains information about chemical potential and stability (hardness) of the system. The hardness (η) and chemical potential (μ) are given the following relations $\eta = (I - A)/2$ and $\mu = -(I + A)/2$, where I and A are the first ionization potential and electron affinity of the chemical species [32]. For the title compound, E_{HOMO}= -5.039 eV, E_{LUMO}= -0.517eV, Energy gap = $E_{HOMO} - E_{LUMO}$ = 4.522 eV, Ionization potential I = 5.039 eV, Electron affinity A = 0.517eV, global hardness η = 2.261eV, chemical potential μ = -2.778 eV, global electrophilicity = $\omega = \mu^2/2\eta$ = 1.7066 eV. Based on HOMO and LUMO energies the global reactive descriptors are listed in Table-4. The negative value of chemical potential reveals the stability of 10HXZ molecule.

TABLE-4
GLOBAL REACTIVE DESCRIPTORS OF 10HXZ MOLECULE CALCULATED ON B3LYP/6-311G (d,p) BASIS SET

Molecular properties	Mathametical description	Energy (eV)
E_{HOMO}	Energy of HOMO	-5.039
E_{LUMO}	Energy of LUMO	-0.517
Energy gap	$\Delta E_g = E_{HOMO} - E_{LUMO}$	4.522
Ionization potential (IP)	$IP = -E_{HOMO}$	5.039
Electron affinity (EA)	$EA = -E_{LUMO}$	0.517
Electronegativity (χ)	$\chi = -1/2(E_{LUMO} + E_{HOMO})$	2.778
Chemical potential (μ)	$\mu = 1/2(E_{LUMO} + E_{HOMO})$	-2.778
Global hardness (η)	$\eta = 1/2(E_{LUMO} - E_{HOMO})$	2.261
Softness (S)	$S = 1/2\eta$	0.2211
Electrophilicity index (ω)	$\omega = \mu^2/2\eta$	1.7066

Natural population analysis: Natural population analysis provides an effective method to calculate atomic charges and electron distribution within a molecule [33]. The net atomic charges of the 10HXZ molecule obtained by natural population analysis and distribution of natural charges are plotted in Fig. 5. The natural load values of 10HXZ molecule are presented in Table-5. All hydrogen atoms in 10HXZ molecule have positive charge only. Hydrogen atom H_{15} (0.3868e) have highest positive charge due to their attachment of heavy electronegative nitrogen atom N_{11} (-0.5906e) which shows highest negative charge and these highest positive and negative natural charges indicating charge delocalization in the molecule. The positive charges are localized on the hydrogen atoms where the charge noticed on the H_7, H_{13} and H_{15} are larger compared to other hydrogen by in natural charges involving hydrogen bonding. The charges at the sites of the C atoms attached to the O atoms C_6 and C_{13} are more positive than other carbon atoms due to the presence of the electron-withdrawing nature of the O atom.

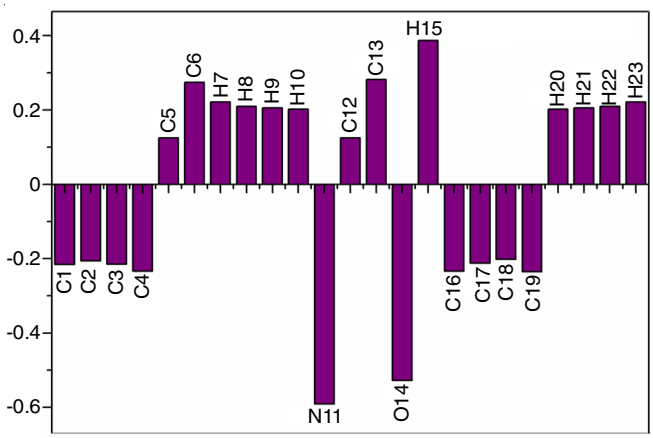

Fig. 5. Natural charges of 10HXZ molecule

TABLE-5
CALCULATED NATURAL CHARGE OF 10HXZ MOLECULE B3LYP/6-311G (d,p) BASIS SET

Atoms	Natural charges	Atoms	Natural charges
C_1	-0.21588	C_{13}	0.28202
C_2	-0.2059	O_{14}	-0.528
C_3	-0.21494	H_{15}	0.3868
C_4	-0.23397	C_{16}	-0.23362
C_5	0.12473	C_{17}	-0.21263
C_6	0.27474	C_{18}	-0.20183
H_7	0.22162	C_{19}	-0.23469
H_8	0.2096	H_{20}	0.20256
H_9	0.20558	H_{21}	0.20574
H_{10}	0.20247	H_{22}	0.20977
N_{11}	-0.59063	H_{23}	0.22178
C_{12}	0.12481		

Natural charges of all carbon atoms are except C_5, C_6, C_{12} and C_{13} due to their attachment with electronegative nitrogen or oxygen atoms.

Fukui function: Fukui indices are, in short, reactivity indices provide information concerning that atoms during a molecule have a large tendency to either loose or accept an electron, which we tend to chemist interpret as that are a lot of susceptible to endure a nucleophilic or an electrophilic attack, respectively. The Fukui function is defined as [34].

$$F = \left(\frac{\delta\rho(r)}{\delta N}\right)r$$

where $\rho(r)$ is the electron density, N is the number of electrons, r is that the external potential. The Fukui function is a local reactivity descriptor which gives the preferred regions where a chemical species will change its density when the number of electrons is modified. Hence, Fukui function indicates the propensity of the electronic density to deform at a given position upon accepting or donating electrons [35,36] and the corresponding condensed or atomic Fukui functions on the j^{th} atom site are given as:

$$F_j^+ = Q_j(N+1) - Q_j(N)$$

$$F_j^- = Q_j(N) - Q_j(N-1)$$

$$F_j^0 = 1/2[Q_j(N+1) - Q_j(N-1)]$$

The electrophilic, nucleophilic and free radical on the reference molecule denoted by the symbol F_j^-, F_j^+, F_j^0 respectively. In the above equations, Q_j is that the atomic charge at the j^{th} atomic site is the neutral (N), anionic (N+1) or (N-1) chemical species. Chattaraj *et al*. [36] have introduced the thought of generalized philicity.

It contains the majority info concerning hitherto well-known completely different global and local reactivity and selectivity descriptor, in additionally to the data concerning electrophilic/ nucleophilic power of a given atomic site during a molecule. Morell *et al*. [37] have recently planned a dual descriptor ΔF(r), which is defined as the difference between the nucleophilic and electrophilic Fukui function and is given by the equation:

$$\Delta F(r) = [F^+(r) - F^-(r)]$$

The site is favoured for a nucleophilic attack whereas dual descriptor ΔF(r)>0 and the site is favoured for an electrophilic attack whereas dual descriptor ΔF(r)<0. According to dual descriptor ΔF(r) give a transparent distinction between nucleophilic and electrophilic attack at a particular site with their sign. That is they provide positive value prone for electrophilic attack. Dual descriptor values are reported in Table-6, according to the condition for dual descriptor, nucleophilic site for in our 10HXZ molecule is C_2, C_3, C_5, C_6, N_{11}, C_{12}, C_{13}, O_{14}, C_{17} and C_{18} are positive values *i.e.* ΔF (r) > 0. Similarly the electrophilic site is C_1, C_4, H_7, H_8, H_9, H_{10}, H_{15}, C_{16}, C_{19}, H_{20}, H_{21}, H_{22} and H_{23} are negative values *i.e.* ΔF(r) < 0. The behaviour of molecule as electrophilic and nucleophilic attack throughout reaction depends on the local behaviour of molecule.

Molecular electrostatic potential: Using molecular electrostatic potential maps, the charge distribution of the molecules can be explained and charge distribution is important since they determine how molecules interact with one another as they point out the reactive sites in the molecule [38,39]. The dissimilar values of the MEP surface represented by different colours in the arrangement such as red surface represents the most electro negative electrostatic potential, blue surface represents the most positive electrostatic potential and green surface represent the zero potential. Potential increases in the order red > orange > yellow > green > blue [40]. In the MEP plot, higher electrostatic potential energy (blue) indicates stronger positive charge which in turn gives the relative absences of electrons and low electrostatic potential (red) indicates the abundance of electrons [41].

In order to visually take into account the most likely sites of the title compound for interaction with nucleophilic and electrophilic species, the MEP was calculated at the optimized geometry level of B3LYP/6-311 G (d,p) and the MEP image shown in Fig. 6. The electrophilic reactivities are visualized in orange colour, indicating the negative regions of the molecule and the regions of the nucleophilic reactivity are coloured in blue, indicating the positive regions of the molecule, as shown in Fig. 6. In this study, the negative potential of the region exceeds the oxazine ring oxygen atom and the positive potential of the region exceeds the phenyl ring hydrogens and oxazine ring NH group. The cloud charge transfer occurs between the range of -5.586e^{-2} and 5.586 e^{-2}.

NMR analysis: The observed ^{13}C and ^{1}H NMR spectra of the 10HXZ molecule in methanol solvent are shown in Figs. 7 and 8. For 10HXZ molecule, the calculated and experimental values of ^{13}C and ^{1}H NMR chemical shifts are listed in Table-7. The B3LYP/GIAO model calculated the absolute isotropic

TABLE-6
USING MULLIKEN POPULATION ANALYSIS: FUKUI FUNCTIONS (f_i+,f_i-, f_i0, f(r))
FOR ATOMS OF 10HXZ MOLECULE AT B3LYP/6-311G (d,p) METHODS

Atoms	Mulliken atomic charges			Fukui functions			
	$q_{(N+1)}$	q_{N0}	$q_{(N-1)}$	f_j+	f_j-	f_j0	f(r)
C_1	-0.062520	-0.092020	-1.119410	0.029498	1.027396	0.528447	-0.997900
C_2	-0.240360	-0.274890	0.189492	0.034535	-0.464380	-0.214920	0.498918
C_3	-0.287650	-0.304000	1.349664	0.016344	-1.653660	-0.818660	1.670003
C_4	-0.157060	-0.205180	-0.423580	0.048123	0.218403	0.133263	-0.170280
C_5	0.226063	0.205176	1.099578	0.020887	-0.894400	-0.436760	0.915289
C_6	-0.027890	-0.022840	0.194016	-0.005050	-0.216850	-0.110950	0.211798
H_7	0.235783	0.184056	0.073812	0.051727	0.110244	0.080986	-0.058520
H_8	0.223082	0.158684	-0.164170	0.064398	0.322855	0.193627	-0.258460
H_9	0.221382	0.159874	-0.337920	0.061508	0.497791	0.279650	-0.436280
H_{10}	0.191297	0.138304	-1.204210	0.052993	1.342517	0.697755	-1.289520
N_{11}	0.078890	-0.024230	-0.115110	0.103123	0.090874	0.096999	0.012249
C_{12}	0.226063	0.205176	1.099578	0.020887	-0.894400	-0.436760	0.915289
C_{13}	-0.027890	-0.022840	0.194016	-0.005050	-0.216850	-0.110950	0.211798
O_{14}	-0.033640	-0.127740	-0.131030	0.094101	0.003290	0.048696	0.090811
H_{15}	0.310479	0.257621	-0.068390	0.052858	0.326015	0.189437	-0.273160
C_{16}	-0.157060	-0.205180	-0.423580	0.048123	0.218403	0.133263	-0.170280
C_{17}	-0.287650	-0.304000	1.349664	0.016344	-1.653660	-0.818660	1.670003
C_{18}	-0.240360	-0.274890	0.189492	0.034535	-0.464380	-0.214920	0.498918
C_{19}	-0.062520	-0.092020	-1.119410	0.029498	1.027396	0.528447	-0.997900
H_{20}	0.191297	0.138304	-1.204210	0.052993	1.342517	0.697755	-1.289520
H_{21}	0.221382	0.159874	-0.337920	0.061508	0.497791	0.279650	-0.436280
H_{22}	0.223082	0.158684	-0.164170	0.064398	0.322855	0.193627	-0.258460
H_{23}	0.235783	0.184056	0.073812	0.051727	0.110244	0.080986	-0.058520

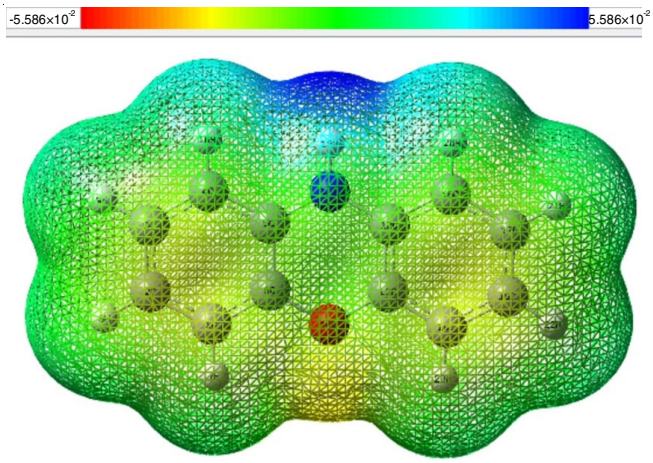

Fig. 6. Molecular electrostatic plot (MEP) of 10HXZ molecule

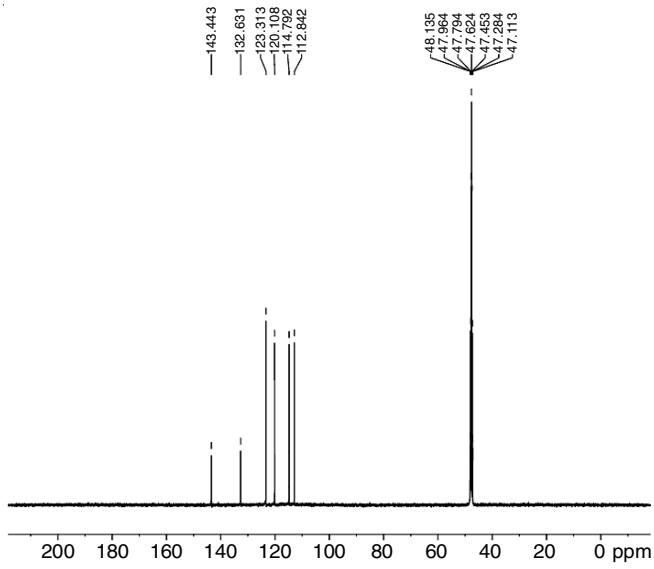

Fig. 7. ^{13}C NMR spectra of 10HXZ molecule

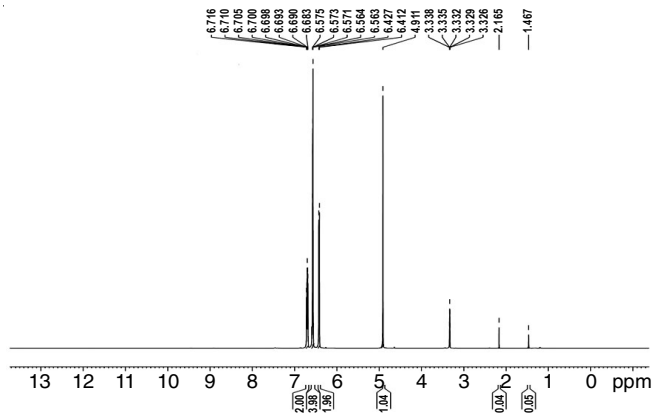

Fig. 8. ^{1}H NMR spectra of 10HXZ molecule

chemical shielding of 10HXZ molecule. Relative chemical shifts were then estimated using the corresponding TMS shielding: σ_{calc} (TMS) is calculated in advance at the same theoretical level. Numerical values of chemical shift $\delta_{pred} = \sigma_{calc}$ (TMS) - σ_{calc} together with calculated values of σ_{calc} (TMS), are given in Table-7.

TABLE-7
CALCULATED AND OBSERVED ^{1}H & ^{13}C NMR SHIFT OF 10HXZ MOLECULE ON B3LYP/6-311G (d,p) BASIS SET

Atoms	Theor.	Exp.	Atoms	Theor.	Exp.
H_7	6.96	6.57	C_1	117.266	114.792
H_8	6.96	6.57	C_2	122.770	120.108
H_9	7.12	6.71	C_3	126.506	123.313
H_{10}	6.66	6.42	C_4	114.231	112.842
H_{15}	4.64	4.91	C_5	135.069	132.631
H_{20}	6.66	6.41	C_6	147.546	142.443
H_{21}	7.12	6.71	C_{12}	135.069	132.631
H_{22}	6.96	6.57	C_{13}	147.546	142.443
H_{23}	6.96	6.57	C_{16}	114.231	112.842
–	–	–	C_{17}	126.506	123.313
–	–	–	C_{18}	122.770	120.108
–	–	–	C_{19}	117.266	114.792

The protons chemical shift occurs with a range of 6.5-8.0 ppm, which usually indicates benzene ring protons. A collection of signals obtained in low field region at 6.41-6.71 ppm corresponds to aromatic protons of 10HXZ moieties and these values are in harmony with the theoretical results. The protons chemical shift occurs with a range of 3.0-5.0 ppm, which usually indicates aromatic NH protons. The singlet peaks at 4.91 ppm are attributed to NH group and the corresponding computed value is 4.64 ppm.

In the ^{13}C NMR, the aromatic carbon signals fall in overlapped areas of the spectrum with the chemical shifts ranging from 100 to 160 ppm in organic molecules [42]. The aromatic carbons in 10HXZ molecule appeared in the deshielded region from 112.842 to 142.443 ppm are in accordance with the calculated results which is 114.231 to 147.546 ppm. The carbon atom C_6 and C_{13} appear highest ^{13}C NMR signals as oxazine ring oxygen atom present in between these two carbon atoms.

Molecular docking: Antimicrobial activity of 10HXZ molecule was determined by the help of molecular docking analysis. For the molecular docking studies of 10HXZ molecule, various microbial active PDBs were selected from protein data bank (RCSB) website. For the identification of title compound antimicrobial activity high resolution three dimension (bactericides and fungicides) PDBs are selected such as 2W7Q, 2X75, 5LM8, 1NMT. The selected proteins are docked with the ligand the following steps are processed. By removing co-crystallized ligands and water molecules, the protein was prepared for docking. The graphical user interface of Auto Dock Tools (ADT) was used to prepare the receptor using a predefined script (add hydrogen, calculate Kolmann charges, save as a PDBQT file). The ligand was prepared for docking by minimizing its energy at the theory level of B3LYP/6-311 G (d,p) and using the ADT script, the ligand was converted to PDBQT. The search area (docking grid box) covered the active site of the enzyme. The size of the box covered the entire active cavity. All calculations of molecular docking were carried out on software Auto Dock-Vina [43]. The low energy binding values indicate the highest affinity of the ligand protein complex. In the present docking analysis, the 10HXZ molecule exhibits significant activity with protein 1NMT, with a binding energy of -6.98 kcal/mol, indicating that 10HXZ molecule could exhibit significant antimicrobial activity against different species

by targeting protein 1NMT. The 10HXZ molecule shares one hydrogen bond with 1NMT protein target as shown in Fig. 9. The hydrogen bond interactions were formed with the residue ARG 423 with the bond distance 2.09 Å. Amino acid ARG 423 associate Hydrogen bond with oxazine ring oxygen atom. The 10HXZ molecule also exhibits significant activity with protein 5LM8 with a binding energy of -6.34 kcal/mol and share two hydrogen bonds with the target protein 5LM8, which is PRO 415 and ASN 568. Amino acids PRO 415, ASN 568 associate Hydrogen bond with oxazine ring oxygen and hydrogen atom. The protein ligand interactions of the title compound 10HXZ molecule with different target proteins are presented in Table-8.

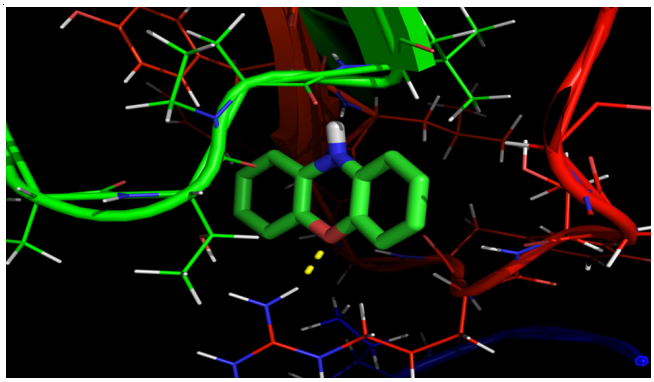

Fig. 9. 10HXZ molecule interact with protein 1NMT

TABLE-8
PROTEIN-LIGAND INTERACTION OF 10HXZ MOLECULE WITH DIFFERENT TARGET PROTEINS

Protein (PDB:ID)	Binding residue	H-bond distance	Incubation constant (μm)	Binding affinity (kcal/mol)
2w7q	ASN 75	2.55	45.24	-5.93
2x75	VAL 98	2.55	51.35	-5.85
5lm8	PRO 415	2.11	22.61	-6.34
	ASN 538	2.62		
1nmt	ARG 423	2.09	7.63	-6.98

Conclusion

10*H*-dibenzo[*b,e*][2,4]oxazine (10HXZ) molecule has been characterized by combined experimental and theoretical quantum chemical calculations using B3LYP/6-311G(d,p) basis set. By comparing calculated chemical shifts and wavenumbers values with experimental value, which show both results almost agreed with each other. NBO analysis indicates the various types of interactions within molecule. The strong intramolecular charge transfer interactions observed between lonepair nitrogen N_{11} to antibonding $\sigma^*(C_{17}–C_{18})$ atoms which leads to the stabalization of 343.83 kcal/mol of the system. The chemical shifts were compared with experimental data in methonal solution, showing a very good agreement both for ^1H & ^{13}C NMR. All the theoretical results show good correspondence with experimental data. In addition, theoretical results from local reactivity descriptors show that the most electrophilic sites are phenyl ring hydrogen H_{10} and H_{20} whereas the most nucleophilic site is N_{11}. The local reactivity descriptors analyses have been used to determine the reactive sites within molecule. Frontier orbital analysis reveals charge transfer interaction takes place within the molecule and the stability of 10HXZ molecule. Docking studies confirms antimicrobial activity of title compound. The above work gives complete structural information and reactive property of 10HXZ molecule with the help of spectroscopic studies.

CONFLICT OF INTEREST

The authors declare that there is no conflict of interests regarding the publication of this article.

REFERENCES

1. O.V. Denisko and A.R. Katritzky, Heterocyclic Compound, Encyclopedia Britannica (1998).
2. Z. Turgut, E. Pelit and A. Köycü, *Molecules*, **12**, 345 (2007); https://doi.org/10.3390/12030345
3. D.S. Zinad, A. Mahal, R.K. Mohapatra, A.K. Sarangi and M.R.F. Pratama, *Curr. Biol. Drug Des.*, **95**, 16 (2020); https://doi.org/10.1111/cbdd.13633
4. M.J. Frisch, G.W. Trucks, H.B. Schlegel, G.E. Scuseria, M.A. Robb, J.R. Cheeseman, G. Scalmani, V. Barone, B. Mennucci, G.A. Petersson, H. Nakatsuji, M. Caricato, X. Li, H.P. Hratchian, A.F. Izmaylov, J. Bloino, G. Zheng, J.L. Sonnenberg, M. Hada, M. Ehara, K. Toyota, R. Fukuda, J. Hasegawa, M. Ishida, T. Nakajima, Y. Honda, O. Kitao, H. Nakai, T. Vreven, J.A. Montgomery Jr., J.E. Peralta, F. Ogliaro, M. Bearpark, J.J. Heyd, E. Brothers, K.N. Kudin, V.N. Staroverov, T. Keith, R. Kobayashi, J. Normand, K. Raghavachari, A. Rendell, J.C. Burant, S.S. Iyengar, J. Tomasi, M. Cossi, N. Rega, J.M. Millam, M. Klene, J.E. Knox, J.B. Cross, V. Bakken, C. Adamo, J. Jaramillo, R. Gomperts, R.E. Stratmann, O. Yazyev, A.J. Austin, R. Cammi, C. Pomelli, J.W. Ochterski, R.L. Martin, K. Morokuma, V.G. Zakrzewski, G.A. Voth, P. Salvador, J.J. Dannenberg, S. Dapprich, A.D. Daniels, O. Farkas, J.B. Foresman, J.V. Ortiz, J. Cioslowski and D.J. Fox, Gaussian 09, Revision C.02, Gaussian Inc., Wallingford CT (2010).
5. T. Sundius, *Vib. Spectrosc.*, **29**, 89 (2002); https://doi.org/10.1016/S0924-2031(01)00189-8
6. H. Yoshida, K. Takeda, J. Okamura, A. Ehara and H. Matsuura, *J. Phys. Chem. A*, **106**, 3580 (2002); https://doi.org/10.1021/jp013084m
7. E.D. Glendening, A.E. Reed, J.E. Carpenter and F. Weinhold, NBO Version 3.1, Theoretical Chemistry Institute and Department of Chemistry, University of Wisconsin, Madison (1998). https://nbo.chem.wisc.edu/nboman.pdf
8. R. Ditchfield, *J. Chem. Phys.*, **56**, 5688 (1972); https://doi.org/10.1063/1.1677088
9. G.M. Morris, R. Huey, W. Lindstrom, M.F. Sanner, R.K. Belew, D.S. Goodsell and A.J. Olson, *J. Comput. Chem.*, **30**, 2785 (2009); https://doi.org/10.1002/jcc.21256
10. R.M. Pearson, C.-H. Lim, B.G. McCarthy, C.B. Musgrave and G.M. Miyake, *J. Am. Chem. Soc.*, **138**, 11399 (2016); https://doi.org/10.1021/jacs.6b08068
11. R.F. Jin, K. Yu, S.Y. Yang and R.B. Huang, *Acta Crystallogr. Sect. E Struct. Rep. Online*, **66**, o3267 (2010); https://doi.org/10.1107/S1600536810047914
12. S.M. Bakalova, A. Gil Santos, I. Timcheva, J. Kaneti, I.L. Filipova, G.M. Dobrikov and V.D. Dimitrov, *J. Mol. Struct. THEOCHEM*, **710**, 229 (2004); https://doi.org/10.1016/j.theochem.2004.07.037
13. A. Dandia, P. Sarawgi, M.B. Hursthouse, A.L. Bingham, M.E. Light, J.E. Drake and R. Ratnani, *J. Chem. Res.*, **2006**, 445 (2006); https://doi.org/10.3184/030823406777980709
14. R.M. Silverstein, G.C. Bassler and T.C. Morril, Spectrometric Identification of Organic Compounds, John Wiley & Sons Inc., Singapore, edn 5 (1991).
15. N.B. Colthup, L.H. Daly and S.E. Wiberly, Introduction of Infrared and Raman Spectroscopy, Academic Press: New York (1975).

16. L.J. Bellamy, The Infrared Spectrum of Complex Molecules, Chapman & Hall: London, edn 3 (1975).
17. J. Coates, ed.: R.A. Meyers, Interpretation of Infrared Spectra, A Practical Approach, John Wiley & Sons Inc., Chichester (2000).
18. D. Sajan, J. Binoy, B. Pradeep, K. Venkata Krishna, V.B. Kartha, I.H. Joe and V.S. Jayakumar, *Spectrochim. Acta A Mol. Biomol. Spectrosc.*, **60**, 173 (2004); https://doi.org/10.1016/S1386-1425(03)00193-8
19. S. Kundoo, A.N. Banerjee, P. Saha and K.K. Chattopadhyay, *Mater. Lett.*, **57**, 2193 (2003); https://doi.org/10.1016/S0167-577X(02)01172-2
20. G. Varsanyi, Assignments of Vibrational Spectra of Seven Hundred Benzene Derivatives, Wiley: New York (1974).
21. M. Kaur, Y.S. Mary, C.Y. Panicker, H.T. Varghese, H.S. Yathirajan, K. Byrappa and C. Van Alsenoy, *Spectrochim. Acta*, **120**, 445 (2014); https://doi.org/10.1016/j.saa.2013.10.032
22. A.J. Abkowicz-Bienko, D.C. Bienko and Z. Latajka, *J. Mol. Struct.*, **552**, 165 (2000); https://doi.org/10.1016/S0022-2860(00)00476-2
23. A.E. Reed, L.A. Curtiss and F. Weinhold, *Chem. Rev.*, **88**, 899 (1988); https://doi.org/10.1021/cr00088a005
24. J.P. Foster and F. Weinhold, *J. Am. Chem. Soc.*, **102**, 7211 (1980); https://doi.org/10.1021/ja00544a007
25. F. Weinhold and C.R. Landis, Valency and Bonding: A Natural Bond Orbital Donor-Acceptor Perspective, Cambridge University Press: New York (2005).
26. L. Padmaja, C. Ravikumar, C. James, V.S. Jayakumar and I. Hubert Joe, *Spectrochim. Acta A Mol. Biomol. Spectrosc.*, **71**, 252 (2008); https://doi.org/10.1016/j.saa.2007.12.019
27. D.A. Dhas, I.H. Joe, S.D.D. Roy and T.H. Freeda, *Spectrochim. Acta A Mol. Biomol. Spectrosc.*, **77**, 36 (2010); https://doi.org/10.1016/j.saa.2010.04.020
28. N. Choudhary, S. Bee, A. Gupta and P. Tandon, *Comput. Theor. Chem.*, **1016**, 8 (2013); https://doi.org/10.1016/j.comptc.2013.04.008
29. B. Kosar and C. Albayrak, *Spectrochim. Acta A Mol. Biomol. Spectrosc.*, **78**, 160 (2011); https://doi.org/10.1016/j.saa.2010.09.016
30. T.A. Koopmans, *Physica*, **1**, 104 (1934); https://doi.org/10.1016/S0031-8914(34)90011-2
31. R.J. Parr, L.V. Szentpaly and S. Liu, *J. Am. Chem. Soc.*, **121**, 1922 (1999); https://doi.org/10.1021/ja983494x
32. R.G. Parr and R.G. Pearson, *J. Am. Chem. Soc.*, **105**, 7512 (1983); https://doi.org/10.1021/ja00364a005
33. A.E. Reed, R.B. Weinstock and F. Weinhold, *J. Chem. Phys.*, **83**, 735 (1985); https://doi.org/10.1063/1.449486
34. P.W. Ayers and R.G. Parr, *J. Am. Chem. Soc.*, **122**, 2010 (2000); https://doi.org/10.1021/ja9924039
35. R.G. Parr and W. Yang, *J. Am. Chem. Soc.*, **106**, 4049 (1984); https://doi.org/10.1021/ja00326a036
36. P.K. Chattaraj, B. Maiti and U. Sarkar, *J. Phys. Chem. A*, **107**, 4973 (2003); https://doi.org/10.1021/jp034707u
37. C. Morell, A. Grand and A. Toro-Labbe, *J. Phys. Chem. A*, **109**, 205 (2005); https://doi.org/10.1021/jp046577a
38. E.Scroco and J. Tomasi, *Quantum Chem.*, **11**, 115 (1979); https://doi.org/10.1016/S0065-3276(08)60236-1
39. P. Politzer and J.S. Murray, eds.: D.L. Beveridge and R. Lavery, Theoretical Biochemistry and Molecular Biophysics: A Comprehensive Survey, In: Electrostatic Potential Analysis of Dibenzo-*p*-dioxins and Structurally Similar Systems in Relation to their Biological Activities, Protein, Academic Press: New York, vol. 2, (1991).
40. V.P. Gupta, A. Sharma, V. Virdi and V.J. Ram, *Spectrochim. Acta A Mol. Biomol. Spectrosc.*, **64**, 57 (2006); https://doi.org/10.1016/j.saa.2005.06.045
41. A.M. Koster, M. Leboeuf and D.R. Salahub, *Theor. Comput. Chem.*, **3**, 105 (1996); https://doi.org/10.1016/S1380-7323(96)80042-2
42. D.L. Pavia, G.M. Lampman, G.S. Kriz and J.R. Vyvyan, Introduction to Spectroscopy, Brooks/Cole: Belmont, USA, edn 4 (2009).
43. O. Trott and A.J. Olson, *J. Comput. Chem.*, **31**, 455 (2010); https://doi.org/10.1002/jcc.21334